Journal of Materials Chemistry C

PAPER

View Article Online
View Journal | View Issue

Cite this: J. Mater. Chem. C, 2014, 2, 8089

Air-stable organic semiconductors based on 6,6′-dithienylindigo and polymers thereof†

E. D. Głowacki,*[a] D. H. Apaydin,[a] Z. Bozkurt,[a] U. Monkowius,[b] K. Demirak,[c] E. Tordin,[a] M. Himmelsbach,[d] C. Schwarzinger,[e] M. Burian,[f] R. T. Lechner,[f] N. Demitri,[g] G. Voss[a] and N. S. Sariciftci[a]

Received 31st March 2014
Accepted 21st July 2014

DOI: 10.1039/c4tc00651h

www.rsc.org/MaterialsC

Herein we report on the synthesis and properties of 6,6′-dithienylindigo (DTI), as well as its solubilized *N*,*N*′-di(*tert*-butoxy carbonyl) derivative (*t*BOC-DTI). *t*BOC-DTI can be electropolymerized and thermally interconverted into films of poly(DTI). Thin films of DTI afford quasi-reversible 2-electron reduction and oxidation electrochemistry, and demonstrate ambipolar charge transport in organic field-effect transistors with a hole mobility of up to 0.11 $cm^2\ V^{-1}\ s^{-1}$ and an electron mobility of up to 0.08 $cm^2\ V^{-1}\ s^{-1}$. Operation of the p-channel shows excellent air stability, with minimal degradation over a 60 day stressing study. Poly(DTI) can be reversibly oxidized and reduced over hundreds of cycles while remaining immobilized on the working electrode surface, and additionally shows a pronounced photoconductivity response in a diode device geometry. This work shows the potential of extended indigo derivatives for organic electronic applications, demonstrating impressive stability under ambient conditions.

Introduction

Indigo and its 6,6′-dibromo derivative, Tyrian Purple, have been used as dyes and pigments for thousands of years by many of the world civilizations.[1] In the 19th century, the high commercial value of indigo dyestuffs encouraged early organic chemists to explore synthesis routes to indigos, and indeed the economic race to develop synthetic indigos was a major impetus behind the development of modern synthetic organic chemistry.[2,3] Recently, it was found that indigo,[4] 6,6′-dibromoindigo,[5] and similar hydrogen-bonded molecules[6,7] show considerable promise for organic electronic applications. In field-effect transistors, indigos show ambipolar operation with mobility in the range 0.01–1.5 $cm^2\ V^{-1}\ s^{-1}$. These materials stand out in particular due to excellent operational stability in air, with minimal performance degradation even after measuring for >1 year.[7] In parallel, there have been extensive studies reported in the literature on semiconducting properties of the closely related building blocks of isoindigos[8,9] and diketopyrrolopyrroles,[10,11] where these chromophores function as electron-accepting units in donor–acceptor type polymers. Indigos themselves were overlooked for such applications, as they are considered to have poor intramolecular π-conjugation.[12] Nevertheless, in crystalline thin films indigos adopt cofacial packing with sufficient transfer integral between neighboring molecules to support charge transport.[7] Formation of highly crystalline films is driven by the interplay of π–π stacking and intra- and intermolecular hydrogen bonding (H-bonding). Very recently in this journal, polymers containing indigo as an acceptor unit in the main chain were reported, with large side chains attached to nitrogens to preserve solubility. These materials show promising n-type behavior with an electron mobility of $\sim 10^{-3}\ cm^2\ V^{-1}\ s^{-1}$.[13] The authors discuss the problematic aspect of the solubilizing chains distorting the planarity of the indigo chromophore. The aim of the study presented here was to develop an efficient synthesis strategy to extend the indigo molecule with well-known organic semiconducting moieties – as a simple building block we use here thiophene – while preserving the H-bonded highly planar indigo unit. To this end, we present two synthesis routes to enable solution-based chemistry while yielding the H-bonded compound in the end. This allows us to test how the indigo moiety can template crystalline growth when functionalized with conjugated units. Additionally, substitution with

[a]Linz Institute for Organic Solar Cells (LIOS), Physical Chemistry, Johannes Kepler University, Linz, Austria. E-mail: eric_daniel.glowacki@jku.at
[b]Institute of Inorganic Chemistry, Johannes Kepler University, Linz, Austria
[c]Materials Science and Engineering, İzmir Katip Çelebi University, Izmir, Turkey
[d]Institute for Analytical Chemistry, Johannes Kepler University, Linz, Austria
[e]Institute for Chemical Technology of Organic Materials, Johannes Kepler University, Linz, Austria
[f]Institute of Physics, Montanuniversitaet Leoben, Franz-Josef-Strasse 18, 8700 Leoben, Austria
[g]Elettra – Sincrotrone Trieste, S.S. 14 Km 163.5 in Area Science Park, 34149 Basovizza, Trieste, Italy

† Electronic supplementary information (ESI) available: $\mathbf{5a_{Vat}}$ details, cyclic FET characteristics, MALDI spectra, X-ray structural data, and computational details. CCDC 1006293. For ESI and crystallographic data in CIF or other electronic format see DOI: 10.1039/c4tc00651h

thiophenes allows facile polymerization. Insolubility of indigos is caused by the interplay of H-bonding and π–π stacking, leading to exceptionally high crystal lattice energies. As a technique to make indigos tractable for synthesis, *N*,*N*′-disubstitution with alkyl or acyl units is used to eliminate H-bonding and distort the planarity of the original indigo molecule. Though such substitution facilitates chemical manipulation, it also interrupts the crystalline packing interactions characteristic of H-bonded indigos and therefore is likely detrimental to transport. In this work we introduce thermolabile protection groups: *t*-butoxy carbonyl (*t*BOC) units. This can render the indigo molecule soluble for chemical manipulation and processing.[14] Afterwards, the *t*BOC groups can be decomposed into gaseous products CO_2 and isobutene by simple heating to temperatures >150° thereby regenerating the planar, H-bonded form of indigo. Using this transient protection technique, we can synthesize 6,6′-dithienylindigo (DTI, **5a**) which can be used to fabricate ambipolar OFETs with $\mu_h = 0.11$ and $\mu_e = 0.08$ $cm^2 V^{-1} s^{-1}$. These OFETs demonstrate impressive stability in air during a 60 day stressing study. The electropolymerized form poly(DTI) is an insulator, however it shows a strong (resistance drop $\sim 10^4$) photoconductivity response in diode geometry. The poly(DTI) can also undergo fully reversible reduction at low potentials (−480 mV *vs.* Ag/AgCl) over hundreds of repeated cycles, making it the first example to our knowledge of a polymer vat dye that preserves its characteristic electrochemistry whilst not dissolving in the electrolyte. The two synthesis routes presented here to achieve extended indigos *via* coupling reactions open up new avenues in using indigo as a functional and stable building block for organic electronic materials.

Results and discussion

Synthesis and crystal structure

Initially, we attempted coupling reactions on **2** directly. However, due to extremely poor solubility of the compound, we were not able to obtain coupling products. Two synthesis approaches that overcome the solubility problem, shown in Scheme 1, were evaluated in order to synthesize compounds **5a**,**b**. In the route shown in the upper part of the scheme, the protect–deprotect route, we synthesize the *t*BOC protected form **4** of Tyrian Purple **2**. Compound **4** is transformed to *t*BOC-DTI **5b** *via* Stille or Suzuki coupling with two equivalents of 2-(tributylstannyl)thiophene or 2-thienyl boronic acid, respectively. In the alternate route, Stille coupling is performed directly on 4-bromo-2-nitrobenzaldehyde **1**, generating **3** with essentially quantitative yield. Compound **3** is then transformed *via* the Baeyer–Drewsen reaction[15] into DTI **5a** with a yield of approx. 25%, which can in turn be protected with *t*BOC to yield **5b**. Material **5a** could be isolated directly from the dried reaction mixture by temperature gradient sublimation in a vacuum to yield highly pure samples. Compound **5b**, on the other hand, was purified by column chromatography to separate it from small amounts of **4** and mono-thienyl coupling byproduct **5c**. Stable aqueous vats of the reduced form $\mathbf{5a_{vat}}$ could be easily prepared using sodium dithionite as the reducing agent despite the hydrophobic thiophene substituents.

Diffraction-quality crystals of **5a** were grown in a temperature-gradient tube furnace under a stream of dry nitrogen with a flow of 2 L min^{-1} using the source material that had previously been purified by sublimation. The source temperature was held at 305 °C and crystals formed in a downstream zone with 110 ± 15 °C. Crystals were measured using synchrotron radiation with a wavelength of 0.7 Å. Experimental details can be found in the ESI.† Projections of the crystal packing structure viewed down the *a* and *b* axes are shown in Fig. 1. The indigo core of **5a** is, like other H-bonded indigos, highly planar, while the thiophene rings are at a torsion angle of 14° relative to the indigo plane. Intermolecular H-bonding occurs along the *a*-direction, with a NH···O = distance of 2.51 Å (Fig. 1b). Typically, this distance for indigo and 6,6′-disubstituted indigos is shorter: ∼2.1 Å. Along the *b*-direction, there is pronounced π–π stacking, with an intermolecular centroid–centroid distance of 4.78 Å (Fig. 1a). The packing arrangement of **5a** is quite unlike any reported indigo crystal structures. Typically, indigos crystallize in a criss-cross arrangement where each molecule forms single hydrogen bonds to four neighbouring molecules, with π–π stacking occurring in the perpendicular direction. The one exception is 6,6′-dichloroindigo, which forms double hydrogen-bonds to two neighbours, leading to linear chains of molecules with adjacent chains propagating in the same direction and a brick-wall type π-stacking structure.[16] The linear-chain *vs.* criss-cross H-bond lattice arrangements are well-known from the work on other H-bonded pigments, where several materials can form both linear-chain and criss-cross polymorphs under certain conditions.[17] Though the linear-chain motif is present in **5a**, the H-bonded sheets of molecules are tilted with respect to each other by 89° along the *c*-axis. The formation of such staggered linear chains is familiar from p-substituted diketopyrrolopyrrole pigments, but has not been observed in indigos before.[18] The close π–π stacking along the *b*-axis probably provides the primary contribution to electronic transport through films of **5a**.

Optical properties

The strong and surprisingly bathochromic absorption in indigoid dyes originates from the so-called indigoid H-chromophore, a cross-conjugated arrangement of electron donor and acceptor groups.[19] Thus, low-energy visible light absorption occurs due to charge transfer from the electron-rich NH groups to the electron-poor carbonyl functions. In order to better understand the absorption and emission data shown in Fig. 2, we conducted DFT calculations to estimate molecular conformation and frontier orbital energies (Fig. 3). The characteristic frontier orbital shapes of the cross-conjugated H-chromophore are the same in compounds **4** and **5** as previously calculated by DFT for other indigos.[20,21] UV-Vis absorption spectra of **5a** and **5b** in DMSO solution are shown in Fig. 2a. Though **5b** is highly soluble in a wide range of organic solvents, DMSO was chosen as a common solvent that also allowed, after heating, dissolution of the deprotected form **5a**. Compound **5a** shows a main HOMO–LUMO transition peak at 580 nm, with a lower-energy shoulder at ∼625 nm, causing the solution to appear deep purple in colour. By way of comparison, indigo in DMSO has a

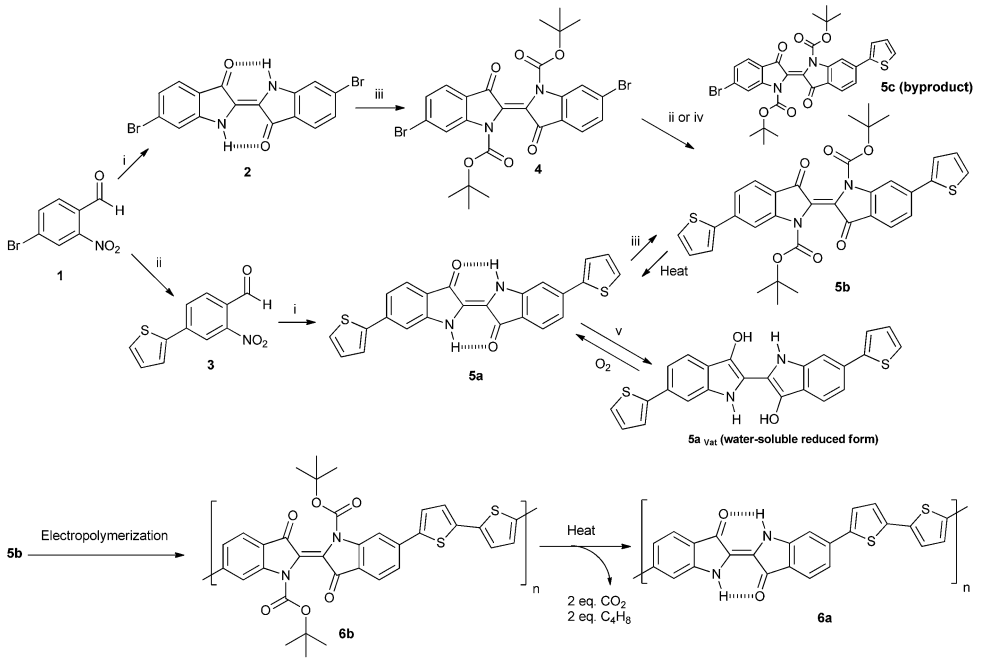

Scheme 1 Two synthesis routes to obtain 6,6′-dithienylindigo, and its polymerized form *via* electrochemical polymerization. (i) acetone, 2M KOH, −5 °C to rt. (ii) $Pd(PPh_3)_4$, 2-(tributylstannyl)thiophene, toluene, reflux under N_2. (iii) Boc_2O, DMAP, THF, rt under N_2. (iv) 2-thienylboronic acid, $Pd(dppf)Cl_2$, 1M K_2CO_3, THF, reflux under N_2. (v) $Na_2S_2O_4$, 2M KOH, heat.

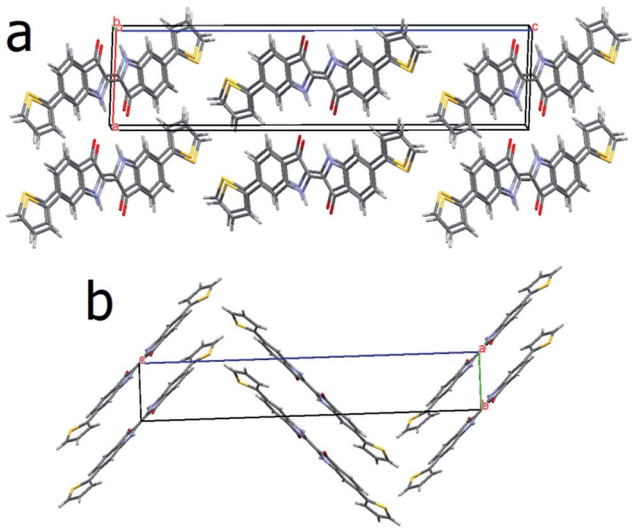

Fig. 1 Crystal structure of DTI (**5a**). (a) A slightly tilted view down the *b*-axis, showing π–π stacking interactions between H-bonded chains of indigos. (b) View down the *a*-axis, showing the direction of propagation of the H-bonded linear chains.

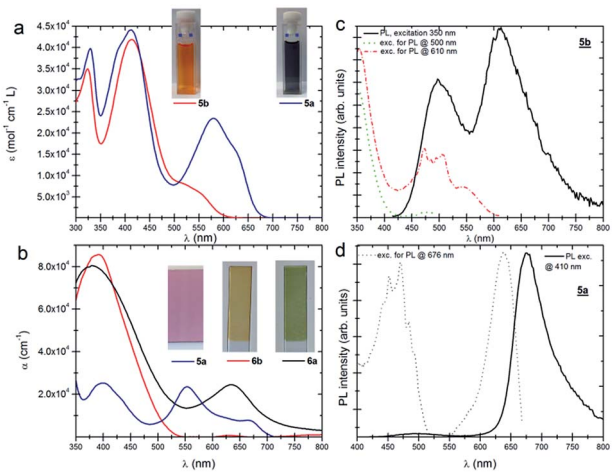

Fig. 2 (a) UV-Vis absorption of **5a**,**b** in DMSO solution. Cuvettes show 0.1 mM solutions. (b) UV-Vis absorption of thin films on ITO glass. (c) Photoluminescence and excitation spectra of **5b** in DMSO solution. (d) Photoluminescence and excitation spectra of **5a** in DMSO.

λ_{max} at 620 nm. It is known that electron-rich substituents in the 6,6′ positions inductively push electron density onto the carbonyl groups,[22–24] decreasing their electron-accepting character and therefore hypsochromically shifting the absorption of the indigoid H-chromophore. It is not surprising that the highly electron-rich thiophene functions shift the absorption so strongly to the blue in the case of **5a**. The protected form of the compound, **5b**, has an even more shifted H-chromophore absorption, with a peak at 540 nm, due to the added contribution of the electron-withdrawing *t*BOC groups, which decrease the electron-donating ability of the nitrogen atoms within the π-system of the H-chromophore. Compound **5b** shows photoluminescence with two distinct peaks, at 500 and 610 nm. The former originates from the chromophore containing the thiophene-phenyl system, as can be deduced from the excitation spectrum. The lower energy luminescence at 610 nm can be attributed to the H-chromophore. The excitation profile for this luminescence band follows that measured in the absorbance

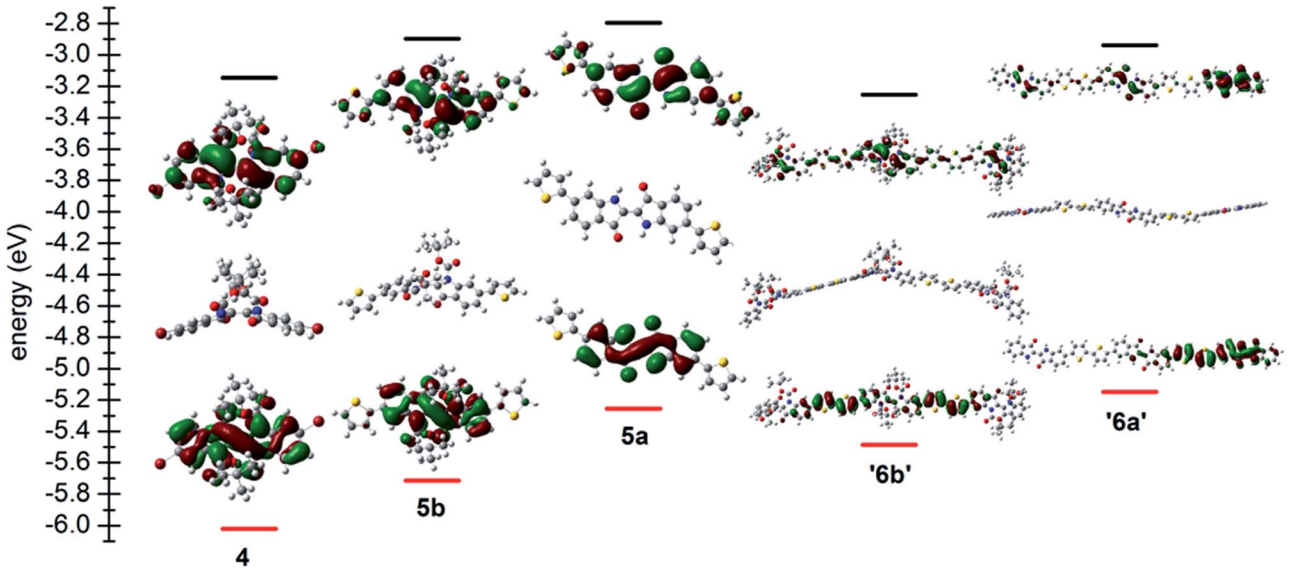

Fig. 3 Optimised ground-state geometries and frontier orbital energies of compounds **4**, and **5a,b** and cut-out segments of polymers **6a** and **6b** obtained by DFT calculations.

spectrum, however with a more distinct fine structure, clearly showing a splitting between higher and lower energy bands that is visible in the case of the unprotected **5a**. The luminescence from **5a**, in solution however, shows one single peak at 676 nm, with the excitation profile fitting closely to the absorbance spectrum. These differences with respect to the protected compound can be rationalized by the fact that *t*BOC substituted compounds are known to be highly distorted with respect to the central double bond,[14] thus the indole–thiophene chromophore can be electronically decoupled from the central H-chromophore. In the rigid and planar **5a**, the electronic structure collapses to lower energy H-chromophore states. Qualitatively consistent with these experimental results are the results of the DFT calculations of frontier orbital energies: the presence of the electron-poor *t*BOC group energetically stabilizes both the HOMO and LUMO orbitals and leads to an increase of the energy gap compared to the unprotected compounds. Fig. 3 shows the relative predicted energy levels as well as ground-state optimized conformations. The predicted DFT band gaps are systematically overestimated, however the qualitative differences, such as the decrease of band gap, upon deprotection (**5b** → **5a**, **6b** → **6a**) reflect what is found experimentally. Also the relative positions of the calculated HOMO and LUMO energy levels follow the same trends found from electrochemical oxidation and reduction onsets, respectively (Table 1).

In the case of thin films, the situation follows what is observed in solutions (Fig. 2b). In evaporated films of **5a**, the absorption splits into a lower energy band with a peak at 670 nm and a higher energy band at 552 nm, the latter having a higher oscillator strength. Thus, the films appear violet in colour and are identical to 6,6′-dibromoindigo (**2**) in appearance. Electropolymerized films with protecting groups (**6b**) are yellow in colour, with only one absorption peak at 398 nm, indicating that the indigoid moieties are highly twisted and thus have limited conjugation. This is also reflected in the DFT conformation calculation. Upon heating and deprotection, the deprotected form of the polymer (**6a**) regains a low energy absorption broad peak at 632 nm, and appears green in colour. Neither polymer film showed any detectable photoluminescence.

Electrochemistry and electropolymerization

Cyclic voltammetry was used to evaluate the electrochemical behaviour of **5a,b** and **6a,b** (Fig. 4). In all cases, 0.1 M tetrabutylammonium hexafluorophosphate in acetonitrile was used as the electrolyte solution, with Ag/AgCl functioning as the quasi-reference electrode, and a Pt foil as the counter electrode. Using

Table 1 Estimations of frontier orbital energy levels

Material	E_{ox} (V *vs.* Ag/AgCl)	E_{red} (V *vs.* Ag/AgCl)	HOMO[a] (eV)	LUMO[b] (eV)	$E_g^{(CV)}$ (eV)	$E_g^{(opt)}$ (eV)
2	1.10	−0.86	−5.8	−3.8	2.0	2.0
5a	0.96	−0.78	−5.6	−3.9	1.7	1.8
5b	1.30	−0.39	−6.0	−4.3	1.7	2.0
6a	1.11	−0.48	−5.8	−4.2	1.6	1.7
6b	1.25	−0.60	−5.9	−4.0	1.9	2.3

[a] $E_{HOMO} = -(E_{[onset,ox.\ vs.\ NHE]} + 4.75)$ (eV). [b] $E_{LUMO} = -(E_{[onset,red.\ vs.\ NHE]} + 4.75)$ (eV).

ferrocene as a standard,[25] we estimated frontier orbital energies for all compounds, summarized in Table 1 together with band gaps calculated from electrochemistry and optical absorption. A worthwhile observation is that the optical band gaps are always equal to or greater than the electrochemically calculated band gaps. In organic semiconducting materials typically this relation is reversed. The exact origin of the unusually small electrochemical gap in indigos, observed in the compounds reported here as well as previously for unsubstituted indigo,[4] is unclear. It may be related to the relatively polar indigo system which can easily undergo oxidation and reduction processes.

We exploited the pendant thiophene groups on DTI **5b** to conduct oxidative polymerization to yield **6b** immobilized on an ITO working electrode. DTI **5b** was dissolved to a concentration of 0.05 M in an electrolyte solution of 0.1 M tetrabutylammonium hexafluorophosphate in acetonitrile. An Ag/AgCl wire functioned as the quasi-reference electrode and a Pt foil served as the counter electrode. The experiments were carried out in a dry N_2 environment. Both potentiodynamic and potentiostatic oxidative polymerization were conducted. Electropolymerization of the monomer **5b** was realized potentiodynamically by cycling potentials between 1600 mV and −500 mV with a scan rate of 50 mV s^{-1} (Fig. 4). Throughout the polymerization a shift in the oxidation potential to higher values was observed which we attribute to the increased ohmic loss as the polymer film grows. *t*BOC-protected poly(DTI) **6b** could then be deprotected by simply heating at 150 °C for 5 minutes, yielding films of poly(DTI) **6a**. Fig. 5c and d show AFM micrographs of poly(DTI) films before and after deprotection. In both cases a crystalline grain-like morphology is visible, quite similar to films of monomer **5a** (Fig. 5a and b) though with significantly lower roughness. Potentiostatic polymerization yielded films with identical morphologies, however significantly thicker (>1 μm) films could be grown since the material was not de-doped by cycling and could be conductive enough to support the growth of thicker films. Neither **6a** nor **6b** could be solubilized for analysis. The structure was confirmed using matrix-assisted laser-desorption ionization (MALDI) mass spectroscopy using samples of thick potentiostatically grown films which could be scratched off the electrode surface as flakes (see ESI† for spectra).

Indigoids are vat dyes, thus upon reduction or oxidation **5a** becomes highly soluble in polar solvents. This causes rapid dissolution of films during cyclic voltammetry and impedes the measurement of respective re-oxidation or re-reduction. In contrast to films of monomer **5a**, the polymerized **6a** showed extraordinary cyclic stability. We conducted 500 scans in acetonitrile under ambient conditions, and found no degradation of the film or change in electrochemical behaviour, the successive scans could be overlaid. Often, repeated reductive electrochemistry in air leads to degradation, however samples of **6a** were highly stable. We attempted measurement in aqueous electrolytes and found that no electrochemical current

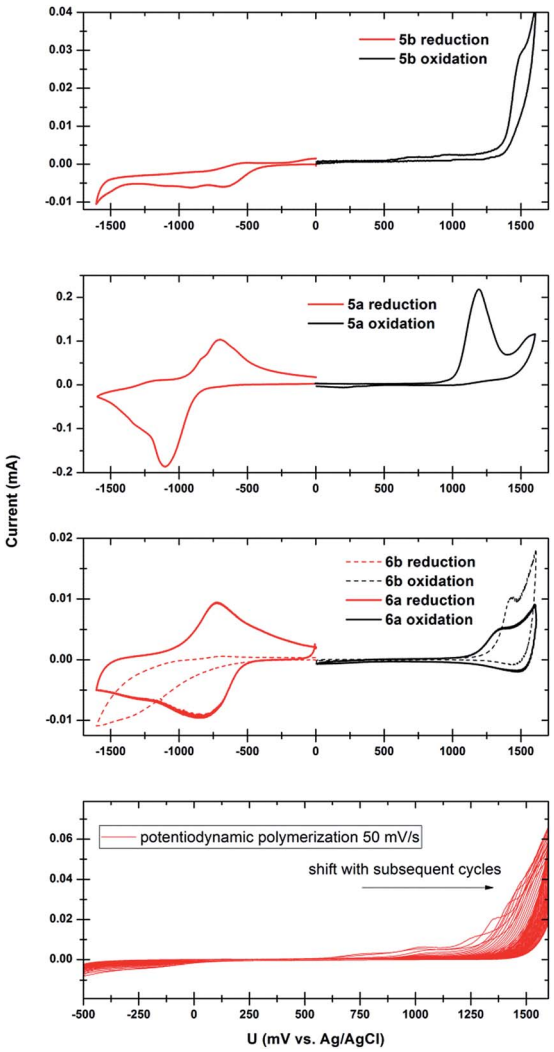

Fig. 4 Comparison of the cyclic voltamograms of **5b** measured in solution, **5a** measured as a film, and polymers **6a** and **6b** as films. A scan rate of 20 mV s^{-1} was used in all cases. The bottom graph shows the potentiodynamic electropolymerization procedure for **5b** → **6b**.

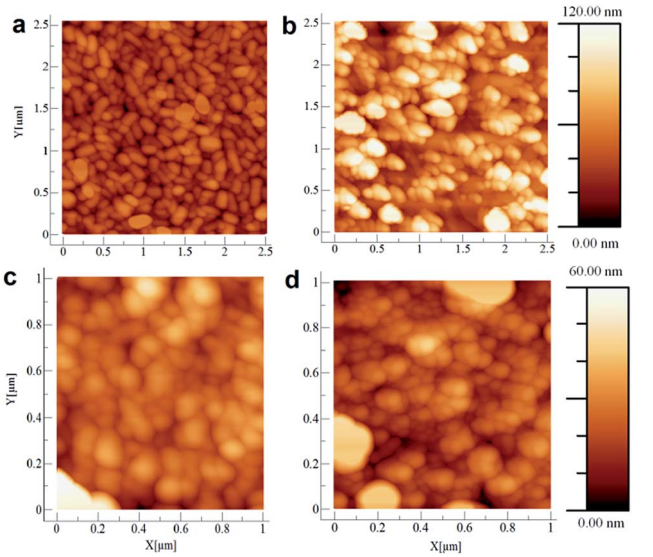

Fig. 5 AFM micrographs of (a) 80 nm of **5a** on ITO, (b) 80 nm of **5a** on AlO_x/TTC, (c) a 140 nm film of **6b** polymerized on ITO, and (d) the same film after heating/deprotection, yielding **6a**.

was measurable, which was attributed to the extreme hydrophobicity of the **6a** film. This has been reported for other conjugated polymers as well. Replacing the electrolyte with the original acetonitrile one immediately yielded the previous electrochemical behaviour. Similarly, monomer **5a** could not be measured with aqueous electrolytes. It was possible, however, to make a basic vat of **5a** using sodium dithionite as the reducing agent. Heating **5a** powder to 85 °C in 2 M KOH with $Na_2S_2O_4$ resulted in a dark orange-coloured vat of the reduced form of **5a** (see spectra in the ESI†). If oxygen was excluded, the vat was stable in its reduced form at least for several days. Admission of air resulted in reoxidation to the neutral **5a** which reprecipitated out of the solution.

Transistors and diodes

DTI (**5a**) could be sublimed in a vacuum to form device-quality films. AFM micrographs of 80 nm of **5a** evaporated with a rate of 0.2 Å s^{-1} on ITO glass and AlO_x/TTC are shown in Fig. 5a and b. Crystalline grains with roughly 100 nm domain size form on ITO, while on the low-surface energy TTC crystallites are considerably larger, with domains of several hundred nanometres. Devices fabricated using **5b** followed by heating to yield **5a** failed to give films, instead isolated crystallites were formed. This behaviour we previously found with other latent indigo pigments.[14] We fabricated organic field-effect transistors using DTI in a device configuration that is known to support transport in H-bonded pigment-forming molecules. A gate electrode of evaporated aluminium is used, with a 32 nm layer of anodized alumina passivated with a 20 nm layer of tetratetracontane ($C_{44}H_{90}$, TTC) functioning as the composite gate dielectric (Fig. 6b).[26] We have reported extensively properties of this gate structure in the past.[7] Next, 80 nm of DTI are evaporated on top with a rate of 0.1 Å s^{-1}. Finally, top Au source/drain contacts are evaporated through a shadow mask to give a W/L of 2 mm/60 μm. Device characteristics were measured in a dry N_2 environment using different V_{DS} values. In all cases the FETs showed ambipolarity (Fig. 6a). A p-type operation is easily obtained with the saturation hole current being independent of V_{DS}, evidencing a low contact resistance for hole injection. From the saturation regime, we calculate $\mu_h = 0.1$ cm^2 V^{-1} s^{-1}. The n-channel, however, was strongly dependent on V_{DS}, therefore a substantial contact resistance existed for electron injection. Once a sufficiently high V_{DS} of 16 V was applied, the n-channel saturates, allowing an estimation of $\mu_e = 0.08$ cm^2 V^{-1} s^{-1}. Application of different contact metals aluminium and silver lowered the contact resistance for electrons, though with a detriment for hole injection. Based on previous observations that indigo and other H-bonded pigments operate stably in air,[6] we conducted stressing/lifetime experiments for DTI FETs, using a pool of eight identical devices. Cyclic measurements of 150 scans were applied in air, with a scan rate of 300 mV s^{-1}. Over 150 cycles the device p-channel shows no fatigue in terms of mobility, on/off ratio, or hysteresis (see ESI†). The n-channel, visible on the first scan, rapidly decays, which is not surprising due to the high energetic position of the LUMO. The n-channel recovers when measured in a N_2 atmosphere, however,

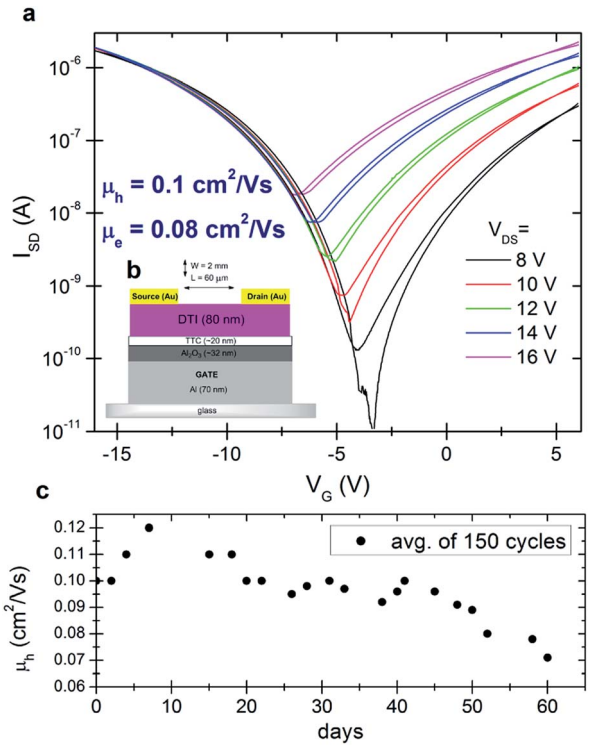

Fig. 6 DTI (**5a**) OFET transfer characteristics (a) with the inset (b) showing the device architecture used for the measurement. (c) OFET device lifetime study – mobility as a function of measurement days in air. Each day 150 cycles were applied.

indicating that O_2 causes electron trapping rather than irreversible degradation of the material. The 150 cycle procedure was repeated over 60 days. Between measurements the samples were stored in an ambient laboratory environment, including room lighting. Over this 60 day stressing study, the hole mobility increases slightly over the first few days, and then gradually decays to 0.07 cm^2 V^{-1} s^{-1} (Fig. 6c).

Diodes using evaporated DTI as well as the poly(DTI) **6a**,**b** were fabricated using ITO as a transparent substrate electrode. In the former case, a 140 nm layer of DTI was evaporated, followed by an aluminium top electrode. For poly(DTI) diodes, a 140 nm film was prepared by potentiodynamic electropolymerization of **5b**, followed by extensive washing with acetonitrile and water to remove residual salts, and finally heating to generate a film of **6a**. An evaporated top electrode of Al or MoO_x/Ag completes the device. Current–voltage characteristics of DTI **5a** and poly(DTI) **6a** diodes are shown in Fig. 7. Films of **6b** were completely insulating in all cases and thus results are not shown. DTI demonstrated essentially no rectification, and relatively low currents. Based on the conductivity of these sandwich geometry devices, the carrier mobility of the majority carrier cannot exceed the 10^{-3} cm^2 V^{-1} s^{-1} range. Irradiation with light from a solar simulator (80 mW cm^{-2}) results in a pronounced photovoltaic effect and also a roughly tenfold increase in conductivity. Considering the markedly higher mobility in FET devices, it is likely that a high trap density exists in this material. This is supported by the

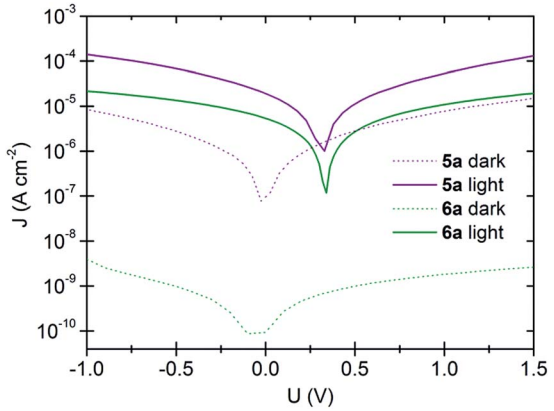

Fig. 7 *J–V* characteristics of ITO/DTI or poly(DTI)/Al devices, measured in the dark or under simulated solar illumination with an intensity of 80 mW cm^{-2}.

photoconductivity effect explained by photogenerated carriers filling trap states. These observations are consistent with the similar disparity between diodes and FET devices reported in other hydrogen-bonded pigment semiconductors, suggesting an important role of traps in this materials class.[27] In the case of poly(DTI) **6a** devices, the effect of photoconductivity is more dramatic. The devices in the dark have a resistivity of ~10 TΩ cm. Irradiation causes an increase in conductivity by 10^4. The high resistivity of the poly(DTI) material is explained by the lack of conjugation along the polymer chain, *i.e.* the indigo units can be seen as interrupting along-chain conduction. The excited state of indigo, however, is known to exist in the *enol* tautomeric form, which indeed supports a mesomeric structure allowing along-chain conjugation (similar to mesomeric structure of $\mathbf{5a_{vat}}$). This latent conjugation phenomenon model was proposed for indigo-containing polymers by Yamamoto.[28] We hypothesize that this could be the reason for the observed photoconductivity.

Experimental

Materials and methods

4-Bromo-2-nitrobenzaldehyde (**1**) was synthesized from 1,4-dibromo-2-nitrobenzene (*Aldrich*) using the regioselective lithiation/formylation reaction reported by Voss *et al.*[29] Compounds **2** (ref. 29) and **4** (ref. 14) were obtained according to published procedures. 1,1′-bis(diphenylphosphino)ferrocene]-dichloropalladium(II) ($Pd(dppf)Cl_2$), tetrakis-triphenylphosphine-palladium(0), 2-tributylstannyl-thiophene and 2-thienylboronic acid were commercially available and used as-received (Aldrich). All solvents were distilled before use. Column chromatography: Merck silica gel 60 (SiO_2; 0.040–0.063 mm). IR [$\bar{\nu}$ in cm^{-1}]: Shimadzu IRTracer-100. UV-Vis: Perkin-Elmer Lambda 950 with a PMT detector. NMR Bruker 300 (^{1}H: 300 MHz; ^{13}C: 75.5 MHz). For ^{13}C experiments: C13APT (Attached Proton Test using the J_{mod} pulse program) was used to assist in peak assignment. MALDI spectra were obtained using a Bruker Autoflex III Smartbeam using linear mode. Samples were prepared by intensive mixing of a small amount of the polymerized film together with an excess of dithranol in a mortar. A small aliquot of the solid mixture was then transferred onto a MALDI target and rubbed in with a spatula. An average of at least 500 spectra was summed up to minimize errors due to the rather rough surface of the solid sample preparation. Electrochemical measurements were carried out in a dry N_2 environment using dry 0.1 M tetrabutylammonium hexafluorophosphate in acetonitrile as an electrolyte. Thin films of the material on ITO functioned as the working electrode, platinum foil was used as the counter electrode, and Ag/AgCl was used as the quasi-reference electrode. Measurements were calibrated against ferrocene. The values of Fc/Fc^+ *vs.* NHE and NHE *vs.* vacuum level used in this work were 0.64 and −4.75 V, respectively.[25] ITO glass slides used for electrochemistry and diode fabrication were cleaned sequentially with acetone, isopropanol, detergent, and DI water, and finally treated with O_2 plasma. Aluminum/aluminum oxide/TTC gate structures were prepared according to reported methods.[30,31]

2-Nitro-4-(2-thienyl)benzaldehyde (3). To a solution of 458 mg (1.9 mmol) of **1** in 60 ml of degassed toluene, 0.6 ml (2.0 mmol) of 2-(tributylstannyl)thiophene was added. After 15 min, 11 mg of tetrakis-triphenylphosphine-palladium(0) was added. The mixture was stirred for 16 h at 110 °C. Evaporation of the solvent gave 500 mg of crude **3**; for analysis a sample was sublimed using a source temperature of 85 °C at a vacuum of 1 × 10^{-6} mbar, to give a bright yellow powder. ^{1}H-NMR ($CDCl_3$): 7.20 (dd, ^3J = 5.0 Hz, ^3J = 3.7 Hz, 1H, 4-$H_{thienyl}$), 7.51 (dd, ^3J = 5.0 Hz, ^4J = 1.0 Hz, 1H, 5-$H_{thienyl}$), 7.57 (dd, ^3J = 3.7 Hz, ^4J = 1.0 Hz, 1H, 3-$H_{thienyl}$), 7.98 (dd, ^3J = 8.1 Hz, ^4J = 1.0 Hz, 1H, 5-H), 8.03 (d, ^3J = 8.1 Hz, 1H, 6-H), 8.30 (d, ^4J = 1.0 Hz, 1H, 3-H), 10.42 (s, 1H, C*H*O). ^{13}C-NMR ($CDCl_3$): 120.9, 126.4, 128.4, 128.7, 128.9, 129.9, 130.5, 140.2, 140.3, 150.5, 187.3. HR ESI-MS: *m*/*z* found for $[M + Na]^+$ 256.0038, *m*/*z* calculated for $[M + Na]^+$ 256.0039.

6,6′-Di(2-thienyl)-indigo (5a). 3 (~1.8 mmol) was dissolved in 65 ml of acetone. After cooling to −5 °C, 120 ml of 2 M KOH was added drop-wise over 2 h. After 16 h stirring at room temperature, the mixture was filtered. The solid was washed with water and ethanol and finally sublimed at 245 °C/1 × 10^{-6} mbar, yielding 77 mg (19%) of **5a** as a purplish powder. IR: among others 3107 (brd, NH), 3105, 3064, 3055 (all vw), 1604, 1575, 1436 (all s). ^{1}H-NMR (DMSO-d_6): 7.51 (dd, ^3J = 5.0 Hz, ^4J = 1.0 Hz, 2H, 3,3′-$H_{thienyl}$), 7.30 (d, ^3J = 8.1 Hz, 2H, 5,5′-H), 7.65–7.68 (6H, 4,4′,7,7′-H and 4,4′-$H_{thienyl}$), 7.71 (d, ^3J = 4.9 Hz, 2H, 5,5′-$H_{thienyl}$), 10.54 (brd s, 2H, NH). HR ESI-MS: *m*/*z* found for $[M + H]^+$ 427.0565, *m*/*z* calculated for $[M + H]^+$ 427.0569.

A sample of **5a** was transformed with $Na_2S_2O_4$/NaOD in D_2O into *leuco N,N′-dideutero-6,6′-di(2-thienyl)-indigo* ($\mathbf{5a_{vat}}$) for NMR analysis according to the method reported by Voss.[32]

^{1}H-NMR (D_2O): 7.08 (m, 2H, 4,4′-$H_{thienyl}$), 7.32–7.40 (4H, 5,5′-H, 3,3′-$H_{thienyl}$), 7.36 (m, 2H, 5,5′-$H_{thienyl}$), 7.49 (d, ^3J = 8.1 Hz, 2H, 4,4′-H), 7.57 (s, 2H, 7,7′-H).

1,1′-Bis(*tert*-butoxycarbonyl)-[6,6′-di(2-thienyl)-indolidene indolyden]-3,3′-dione [(bis-*t*BOC-6,6′-di(2-thienyl)-indigo; 5b], and the mono-substituted byproduct 1,1′-bis(*tert*-butyoxycarbonyl)-[6-(2-thienyl)-6′-bromo]-indolidene indolyden]-3,3′-dione [bis-*t*BOC-[6-(2-thienyl)-6′-bromo]-indigo; 5c]. Procedure

1 – *Suzuki* coupling:[33] To a degassed solution of 440 mg (0.71 mmol) of **4** in 50 ml of dimethoxyethane, 227 mg (1.8 mmol) of 2-thienyl-boronic acid was added. After 10 min stirring under N_2, 80 mg (0.1 mmol) of Pd(dppf)Cl_2 was added. Then the mixture was heated for 30 min to slight reflux (T_{bath} 90 °C) and 2 ml of 1 M K_2CO_3 was added. Stirring and heating were continued for 1 h, and then the mixture was set aside at room temperature for 16 h. Diethylether (200 ml) was added and the organic layer was washed with water. After evaporation of the solvent, the residue (570 mg, red oil) was chromatographed on silica gel with cyclohexane/AcOEt (9 : 1). Starting materials **4** (120 mg, 44%, $R_f = 0.48$), **5b** (130 mg, 29%, $R_f = 0.21$) and **5c** (110 mg, 23%, $R_f = 0.32$) were isolated as red solids. Recrystallization from cyclohexane gave the analytically pure products.

Procedure 2 – *Stille* coupling:[34] 496 mg (0.8 mmol) of **4** was dissolved in 60 ml of dry toluene. The mixture was degassed by 15 min N_2 bubbling. Next, 0.6 ml (2 mmol) of 2-(tributylstannyl) thiophene was added and N_2 bubbling was continued for 15 min. After addition of 9.2 mg (0.008 mmol) of tetrakis-triphenylphosphine palladium(0), the mixture was stirred for 16 h at 90 °C. After evaporation of volatile products, the residue was chromatographed on silica gel (Cy/AcOEt, 9 : 1).

Starting materials 4 (92 mg, 18%), 5b (170 mg, 33%), 5c (120 mg, 23%)

5b. IR: among others 3107, 3074 (all vw), 2974, 2927 (all w), 1703, 1600, 1435, 1147 (all s). – ^{1}H-NMR ($CDCl_3$): 1.70 (s, *t*BOC CH_3, 18H), 7.17 (dd, $^3J = 5.0$ Hz, $^3J = 3.6$ Hz, 2H, 4,4′-$H_{thienyl}$), 7.44 (dd, $^3J = 5.0$ Hz, $^4J = 0.9$ Hz, 2H, 5,5′-$H_{thienyl}$), 7.49 (dd, $^3J = 8.0$ Hz, $^4J = 1.4$ Hz, 2H, 5.5′-H), 7.52 (dd, $^3J = 3.6$ Hz, $^4J = 0.9$ Hz, 2H, 3,3′-$H_{thienyl}$), 7.78 (d, $^3J = 8.0$ Hz, 2H, 4,4′-H), 8.33 (d, $^4J = 1.4$ Hz, 2H, 7,7′-H). ^{13}C-NMR ($CDCl_3$): 28.2 (*t*BOC CH_3), 113.5 (7,7′-C), 121.6, 124.7, 125.4, 127.2, 128.6 (4,4′- and 5,5′-C, and 3,3′-, 4,4′- and 5,5′-$C_{thienyl}$) – only the signals of those carbon atoms attached to hydrogens are given. HR ESI-MS: *m*/*z* found for $[M + H]^+$ 627.1611, *m*/*z* calculated for $[M + H]^+$ 627.1618.

5c. (Mono-thienyl byproduct). IR: among others 3120 (vw), 2972, 2924 (all w), 1734, 1672, 1600, 1421, 1141 (all s). ^{1}H-NMR ($CDCl_3$): 1.64 (s, *t*BOC CH_3, 9H), 1.69 (s, CH_3, 9H), 7.16 (dd, $^3J = 5.1$ Hz, $^3J = 3.7$ Hz, 1H, 4-$H_{thienyl}$), 7.37 (dd, $^3J = 8.1$ Hz, $^4J = 1.6$ Hz, 1H, 5′-H), 7.44 (dd, $^3J = 5.1$ Hz, $^4J = 1.5$ Hz, 1H, 3-$H_{thienyl}$), 7.50 (dd, $^3J = 8.0$ Hz, $^4J = 1.0$ Hz, 1H, 5-H), 7.52 (dd, $^3J = 3.7$ Hz, $^4J = 1.5$ Hz, 1H, 5-$H_{thienyl}$), 7.63 (d, $^3J = 8.1$ Hz, 1H, 4′-H), 7.78 (d, $^3J = 8.0$ Hz, 1H, 4-H), 8.30 (s, 1H, 7′-H), 8.31 (s, 1H, 7-H). HR ESI-MS: *m*/*z* found for $[M + H]^+$ 623.0859, *m*/*z* calculated for $[M + H]^+$ 623.0846.

Conclusions

We have presented synthesis routes to obtain an extended indigo derivative, 6,6′-dithienylindigo (DTI), for application as an organic semiconductor. We utilize the latent pigment technique of introducing thermolabile solubilizing groups, which allows chemical manipulation of the otherwise insoluble indigo moiety. DTI shows promising ambipolar transport behaviour in FET devices, with impressive operational stability in air. By electropolymerization we could produce poly(DTI). This semi-conjugated polymer with indigo in the main chain shows interesting photoconductivity behaviour and suggests that the *enolic* structure might lead to conjugation. The poly(DTI) shows excellent stability during electrochemical cycling, with a notably low reduction potential. The results presented here show the promise that extended indigos and indigo-based polymers can have for organic electronics.

Acknowledgements

We are grateful for support from the Austrian Science Foundation, FWF, within the Wittgenstein Prize of N. S. Sariciftci Solare Energie Umwandlung Z222-N19 and the Translational Research Project TRP 294-N19 "Indigo: From ancient dye to modern high-performance organic electronic circuits".

Notes and references

1 M. Seefelder, *Indigo in culture, science, and technology, ecomed*, Landsberg, Germany, 2nd edn, 1994.
2 H. Schmidt, *Chem. Unserer Zeit*, 1997, **31**, 121–128.
3 E. Steingruber, *Indigo and Indigo Colorants in Ullmann's Encycl. Ind. Chem.*, 2007.
4 M. Irimia-Vladu, E. D. Głowacki, P. A. Troshin, G. Schwabegger, L. Leonat, D. K. Susarova, O. Krystal, M. Ullah, Y. Kanbur, M. A. Bodea, V. F. Razumov, H. Sitter, S. Bauer and N. S. Sariciftci, *Adv. Mater.*, 2012, **24**, 375–380.
5 E. D. Głowacki, L. Leonat, G. Voss, M.-A. Bodea, Z. Bozkurt, A. M. Ramil, M. Irimia-Vladu, S. Bauer and N. S. Sariciftci, *AIP Adv.*, 2011, **1**, 042132–042137.
6 E. D. Głowacki, M. Irimia-Vladu, M. Kaltenbrunner, J. Gąsiorowski, M. S. White, U. Monkowius, G. Romanazzi, G. P. Suranna, P. Mastrorilli, T. Sekitani, S. Bauer, T. Someya, L. Torsi and N. S. Sariciftci, *Adv. Mater.*, 2013, **25**, 1563–1569.
7 E. D. Głowacki, G. Voss and N. S. Sariciftci, *Adv. Mater.*, 2013, **25**, 6783–6800.
8 E. Wang, W. Mammo and M. R. Andersson, *Adv. Mater.*, 2014, **26**, 1801–1826.
9 R. Stalder, J. Mei, K. R. Graham, L. A. Estrada and J. R. Reynolds, *Chem. Mater.*, 2014, **26**, 664–678.
10 S. Qu and H. Tian, *Chem. Commun.*, 2012, **48**, 3039–3051.
11 C. B. Nielsen, M. Turbiez and I. McCulloch, *Adv. Mater.*, 2012, **25**, 1859–1880.
12 M. J. Robb, S.-Y. Ku, F. G. Brunetti and C. J. Hawker, *J. Polym. Sci., Part A: Polym. Chem.*, 2013, **51**, 1263–1271.
13 C. Guo, B. Sun, J. Quinn, Z. Yan and Y. Li, *J. Mater. Chem. C*, 2014, **2**, 4289–4296.
14 E. D. Głowacki, G. Voss, K. Demirak, M. Havlicek, N. Sunger, A. C. Okur, U. Monkowius, J. Gąsiorowski, L. Leonat and N. S. Sariciftci, *Chem. Commun.*, 2013, **49**, 6063–6065.
15 A. Baeyer and V. Drewsen, *Chem. Ber.*, 1882, **15**, 2856–2864.
16 P. Susse and R. Wasche, *Naturwissenschaften*, 1978, **65**, 157.
17 E. F. Paulus, F. J. J. Leusen and M. U. Schmidt, *CrystEngComm*, 2007, **9**, 131.
18 Z. Hao and A. Iqbal, *Chem. Soc. Rev.*, 1997, **26**, 203.
19 W. Lüttke, H. Hermann and M. Klessinger, *Angew. Chem., Int. Ed. Engl.*, 1966, **5**, 598–599.

20 A. Amat, F. Rosi, C. Miliani, A. Sgamellotti and S. Fantacci, *J. Mol. Struct.*, 2011, **993**, 43–51.
21 D. Jacquemin, J. Preat, V. Wathelet and E. A. Perpète, *J. Chem. Phys.*, 2006, **124**, 74104.
22 P. W. Sadler, *J. Org. Chem.*, 1955, **21**, 316–318.
23 P. W. Sadler and R. L. Warren, *J. Am. Chem. Soc.*, 1956, **78**, 1251–1255.
24 H. Zollinger, *Color Chemistry. Syntheses, Properties and Applications of Organic Dyes and Pigments*, Wiley-VCH, Weinheim, 3rd edn, 2003, vol. 43.
25 C. M. Cardona, W. Li, A. E. Kaifer, D. Stockdale and G. C. Bazan, *Adv. Mater.*, 2011, **23**, 2367–2371.
26 E. D. Głowacki, M. Irimia-Vladu, S. Bauer and N. S. Sariciftci, *J. Mater. Chem. B*, 2013, **1**, 3742–3753.
27 E. D. Głowacki, L. Leonat, M. Irimia-Vladu, R. Schwödiauer, M. Ullah, H. Sitter, S. Bauer and N. Serdar Sariciftci, *Appl. Phys. Lett.*, 2012, **101**, 023305.
28 T. Yamamoto and K. Kizu, *J. Phys. Chem.*, 1995, **99**, 8–10.
29 G. Voss and H. Gerlach, *Chem. Ber.*, 1989, **122**, 1199–1201.
30 A. I. Mardare, M. Kaltenbrunner, N. S. Sariciftci, S. Bauer and A. W. Hassel, *Phys. Status Solidi*, 2012, **209**, 813–818.
31 M. Kraus, S. Richler, A. Opitz, W. Brütting, S. Haas, T. Hasegawa, A. Hinderhofer and F. Schreiber, *J. Appl. Phys.*, 2010, **107**, 094503.
32 G. Voss, *Color. Technol.*, 2006, **122**, 317–323.
33 A. Suzuki, *J. Organomet. Chem.*, 1999, **576**, 147–168.
34 J. K. Stille, *Angew. Chem., Int. Ed.*, 1986, **25**, 508–524.